PAPER

Check for updates

Study of conductive nerve conduits for anti-inflammatory and antioxidant effects

Runtian Xu, †[a] Hanping He,†[b] Huan Deng,[a] Yuehan Dong,[a] Xiangjie Wu,[a] Zinuo Xia,[a] Yang Zhou,[a] Lin Yang,[a] Zhijun Huang,[a] Wenjin Xu, [a] Peihu Xu *[a] and Haixing Xu *[a]

Replacing autologous nerve grafts with nerve conduits is the prevailing direction for the treatment of peripheral nerves, though the repair of hollow nerve conduits remains unsatisfactory. In this study, cysteinylated zein (L-Zein) was prepared through a disulfide exchange reaction between the disulfide bonds of cysteine (Cys) and those of zein (Zein). Subsequently, electrospinning was utilized to fabricate hollow nerve conduits loaded with berberine (BBR) by means of hydrogen bonding and physical encapsulation. Hydrogels were prepared by ionic cross-linking of Zein with pectin (Pec), and were subsequently loaded with melatonin (MT) and graphene oxide (GO) through physical adsorption and encapsulation. A hydrogel was then injected into a hollow catheter to form a hydrogel composite nerve conduit (L-ZBZPGM). The hydrogels exhibited a continuous porous network structure with pore size distribution between 100 and 200 μm. Most of the hydrogels exhibited porosity exceeding 70% and the compressive modulus was 0.42 ± 0.025 MPa. A hydrogel exhibited a residual mass ratio of $35.15\% \pm 1.87\%$ at the end of the 30 d degradation period, achieved peak release on day 18 with a release rate of $83.31\% \pm 3.64\%$, and had an electrical conductivity of $1.23 \pm 0.482 \times 10^{-3}$ S cm^{-1}, meeting the requirements for nerve repair. The lack of cytotoxicity and the anti-inflammatory and antioxidant properties of L-ZBZPGM were demonstrated using RSC96 cells and Raw264.7 cells. Additionally, through electrical stimulation experiments, it was proven that the addition of GO can promote the proliferation of nerve cells. The biological materials used in this study are of simple composition, and their degradation products may have a minimal impact on the microenvironment. The findings suggested that L-ZBZPGM was more conductive to peripheral nerve regeneration.

1. Introduction

Peripheral nervous injury (PNI) is a major clinical issue, affecting over one million individuals worldwide each year.[1] It is often caused by trauma and can lead to the loss of motor or sensory function. In severe cases, PNI results in long-term disability and reduces quality of life.[2] PNI is categorized into two primary groups: nondegenerative and degenerative. Non-degenerative disease refers to PNI without axonal loss, while degenerative disease pertains to PNI with axonal loss.[3] Although human peripheral nerves possess the capacity for regeneration post-injury, the natural regeneration process is inherently limited and insufficient for full functional recovery.

Nerve guide catheters (NGCs) are widely used as alternatives to autografts in nerve repair. They serve as bridges between damaged nerve ends, facilitating regeneration by providing a pathway, preventing intrusion of peripheral connective tissues and scarring, and supporting axonal growth along the conduit.[4–6] It is imperative that NGC materials exhibit no cytotoxicity or histotoxicity and provoke minimal to no inflammatory response. Therefore, researchers have explored various synthetic and naturally biocompatible polymers such as polycaprolactone, collagen, and carboxymethyl chitosan for the development of NGCs for nerve repair.[7,8] Nerve regeneration failure between the distal and proximal ends may transpire due to the inadequate nutrient provision within the hollow conduit. Consequently, a prevalent approach to augment nerve repair involves filling the catheter with a nutrient-rich hydrogel, potentially containing drugs, that fosters a microenvironment conducive to nerve regeneration.[9]

Hydrogels are cross-linked three-dimensional porous networks of hydrophilic polymers that swell but do not dissolve when exposed to water, exhibiting properties closely akin to those of natural tissues.[10] Their porous structure makes them particularly suitable for use as slow-release carriers for topical drugs. However, it is imperative that hydrogels possess

[a]Department of Pharmaceutical Engineering, School of Chemistry, Chemical Engineering, and Life Sciences, Wuhan University of Technology, Wuhan, 430070, China. E-mail: xhx040328@whut.edu.cn; whutxph68@126.com

[b]Department of Radiation Oncology, Hubei Cancer Hospital, Wuhan, 430079, China

† These authors contributed equally to this work.

Paper

mechanical properties comparable to those of the site they are intended to regenerate; failure to do so may result in mechanical degradation of the scaffold or damage to the surrounding tissue.[11] Furthermore, hydrogels can be employed within nerve conduits to provide essential nutrients for nerve repair, their porous structure facilitating nerve cell migration and proliferation.[12–14]

The design of biomaterials for immunomodulation has recently garnered significant attention as a vital approach to argument tissue regeneration.[15,16] Zein, a protein derived from maize protein powder, is aggregated in maize *via* disulfide bonds and possesses a molecular weight of approximately 25–35 kDa.[17] This plant protein exhibits low immunogenicity and a high potential for *in vivo* degradation.[18–20] However, the abundance of non-polar amino acids in zein limits its modification and broader industrial application in medicine.[21] This study employs L-cysteine as a reducing agent to break disulfide bonds both within and between protein molecules, thereby promoting sulfhydryl–disulfide exchange reactions for protein modification. The hydrolysis of zein proteins based on their amino acid composition significantly alters their structure, thus enhancing their functional properties.[22,23] The integration of modified corn alcohol soluble proteins during the spinning process to prepare nerve conduits renders these conduits more conducive for cell adhesion and proliferation.[24]

Pectin (Pec) is a polysaccharide and polyanion derived from citrus fruit cell walls, consisting of α1-4 glycosidic bond-linked D-galacturonic acid units. It is classified into high and low methoxyl pectins based on the degree of methylation.[25] While Pec inherently possesses limited thermal stability and mechanical properties, these can be augmented when integrated with other biopolymers.[26,27]

Electrical stimulation has been demonstrated to facilitate the recovery of damaged peripheral nerves. As a result, the integration of conductive materials into the components used in the fabrication of nerve conduits can augment their therapeutic efficacy. Electrically stimulated hydrogels present promising scaffolds for nerve repair, necessitating further research and development.[28] Graphene oxide (GO) exhibits superior electrical conductivity, dispersibility, and biocompatibility. The incorporation of GO into hydrogels provides a platform for electrical stimulation, which can enhance the bioactivity and mechanical attributes of the scaffold. This modification fosters a more favorable microenvironment for nerve regeneration.[29–32]

Melatonin (MT) is an indoleamine synthesized not only by the pineal gland but also by numerous other organs. It plays a pivotal role in exerting circadian effects, regulating reproductive functions, and exhibiting free radical scavenging and antioxidant activities.[33] Notably, MT enhances Schwann cell proliferation following peripheral nerve injury, promotes nerve regeneration, and reactivates motor end plates in muscles. Both experimental and clinical studies have demonstrated that MT has a positive impact on various pathologies associated with mitochondrial dysfunction.[34–36] It has been established that MT can bolster mitochondrial autophagy through the enhancement of Parkin expression, he eradication of mitochondrial reactive

oxygen species *in vivo*, and the removal of elements that hinder autophagic flux. These mechanisms work to reinstate autophagic flux and contribute to the repair of peripheral nerve.[37] Berberine (BBR), an isoquinoline alkaloid, is noted for its wide range of biological activities including antioxidant, anti-inflammatory, anticancer, immunomodulatory, and antimicrobial effects. This makes it a promising agent in treating neuroinflammation, as it effectively modulates inflammation triggered by infections, toxins, aging, or ischemia-reperfusion through various signaling pathways.[38,39] Moreover, BBR mitigates neuroinflammatory responses by reducing the production of proinflammatory cytokines in microglia. Notably, BBR has also been shown to partially alleviate cognitive dysfunction induced by LPS by diminishing its neuroinflammatory properties.[40]

In summary, this study proposes the modification of Zein with Cys to create an amphoteric material. This is then electrostatically spun with BBR loaded with L-Zein to fabricate hollow nerve conduits possessing anti-inflammatory properties. Subsequently, Pec, Zein, GO, and MT are reacted to form a conductive hydrogel with antioxidant effects. The resulting drug-carrying hydrogel is then injected into the hollow nerve conduit. The resulting a conductive drug-carrying nerve conduit with both anti-inflammatory and antioxidant effects. Remarkably, this is achieved without the use of cross-linking agents, leading to reduced cytotoxicity. The final product exhibits excellent mechanical properties, as well as drug-carrying, drug-releasing, and degradation capabilities. To our knowledge, there are no prior report on this subject. Our findings suggest that these conductive drug-loaded nerve conduits hold potential for application in the repair of peripheral nerve injuries.

2. Materials and methods

2.1 Materials

Zein (from corn), L-cysteine, pectin, berberine, melatonin, and potassium oleate were obtained from Aladdin Chemistry Co, Ltd. The materials obtained from China include phosphate buffer (0.1 mol L^{-1}, pH 7.4), Dulbecco's modified Eagle's medium (DMEM), penicillin/streptomycin solution, Cell Counting Kit-8 (CCK-8), paraformaldehyde, MitoTracker. Red CMXRos, Triton X-100, and DiI fluorophores were sourced from Boster Biological Technology Co. Ltd. (China). The serum from the donor horse was obtained from Zhejiang Tianhang (China). Fetal bovine serum (FBS) and 4′,6-diamidino-2-phenylindole (DAPI) were procured from Beyotime. Rat schwann cell line 96 (RSC96) and Murine leukemia virus-induced monocytic macrophage cell line (Raw264.7) cells were sourced from the China Center for Type Culture Collection, Wuhan, China.

The study utilized the following instruments: an Agilent 1100 high-performance liquid chromatograph (USA), an Olympus CX31 optical microscope (Japan), a JEOL JEM2100F transmission electron microscope (Japan), a Thermo 6700 FTIR spectrometer (USA), and a JEOL JSM-IT300 scanning electron microscope (Japan). The apparatus included a SANS CMT6503 microcomputer-controlled electronic universal testing machine (MTS, China), a 5601-Y four-point probe resistivity meter

(Quatek, China), a MTHYH-C2000-T constant temperature shaker (Loki, China), and a Nikon Eclipse C1 fluorescence inverted microscope (Nikon, Japan).

2.2 Preparation and characterization of nerve conduits

L-Zein was synthesized following a previously established method,[41] where 1 g of potassium oleate was dissolved in 100 mL of deionized water, followed by the addition and thorough mixing of 3 g of Zein. Cys (0.1 mmol g^{-1}) was introduced to the Zein-potassium oleate system, and the mixture was reacted in a water bath at 37 °C for 30 minutes. The mixed solution was dialyzed in a 3500 Da MWCO dialysis bag using deionized water for 72 hours to eliminate by-products. Freeze-dry the protein samples using a freeze-dryer and set aside.

L-Zein/BBR (L-ZB) nerve conduits were prepared from a previously reported study.[42] L-Zein (1.5 g) was weighed, 80% ethanol solution (10 mL) was added and magnetically stirred until complete dissolution, and different concentrations of BBR (5, 10 and 20 μmol) were added. The spinning solution was aspirated with a 5 mL syringe and loaded with a 20 – gauge spinning needle, and the fibers were received with a catheter receiving device to form a catheter. Electrostatic spinning parameters include a push injection speed of 0.25 mm min^{-1}, a positive voltage of 17 kV, a negative voltage of −5 kV, and a receiving distance of 10 cm. Post-spinning, fibers were oven-dried at 120 °C for 6 hours, with catheters stored in drying dishes for future use. The nerve catheters containing different BBR concentrations were categorized into BBR1, BBR2 and BBR3.

Fourier transform infrared spectroscopy (FTIR) was used to confirm the structural configuration of L-Zein in the 500–4000 cm^{-1} spectral range. In order to gain insight into the chemical composition of the nerve conduits, the aforementioned methodology was employed for a detailed analysis.

A scanning electron microscope (SEM) was employed to observe the spatial structure of the nerve conduits. Subsequently, the samples were subjected to cross-sectioning and sputter coating with gold, after which they were scanned for observation. The mean pore size was determined using the ImageJ software program.

The water contact angle of the nerve conduits was determined prior to and following modification through a contact angle tester.

The tensile modulus of nerve conduits was determined utilizing a microcomputer-controlled electronic universal testing machine. Catheters measuring 20 mm in length and 10 mm in width were fabricated and evaluated for mechanical properties at room temperature under a tensile force of 10 N, with a tensile and compression rate of 1 mm min^{-1}.

The characterization of the drug loading of BBR was conducted in 5 mL centrifuge tubes. The nerve catheters, prepared by the addition of varying concentrations of BBR, were placed in 3 mL of PBS. Centrifuge tubes were shaken in a thermostatic oscillator at 100 rpm and 37 °C for 30 minutes. The drug solution concentration was measured using high-performance liquid chromatography (HPLC). The drug loading of BBR was determined using the formula:

$$\text{Drug loading} = \frac{W_c - W_v}{W_c} \times 100\%$$

where W_c was the total BBR content and W_v was the total BBR content in the supernatant.

The degradation and drug release of nerve conduits were assessed in vitro using a phosphate-buffered saline (PBS) solution with lysozyme. Each nerve conduit was individually weighed and submerged in phosphate-buffered saline (PBS, pH 7.4) with lysozyme (1 mg mL^{-1}) at 37 °C, oscillating at 100 rpm. At specific intervals, 1 mL of the degraded solution was analyzed for BBR concentration using high-performance liquid chromatography (HPLC). After each removal, an equivalent volume of PBS was added. The nerve conduits were extracted from the medium every two days, rinsed twice with deionised water to eliminate surface-adsorbed ions, and subsequently freeze-dried. The dry weight of each sample following the incubation period was recorded as M_t, with the initial weight recorded as M_0.

The residual mass ratio was determined using the formula:

$$\text{Residual mass ratio}(\%) = \frac{M_t}{M_0} \times 100\%$$

The cumulative drug release was determined using the following equation.

$$\text{Cumulative drug release}(\%) = \frac{W_t}{W_0} \times 100\%$$

The cumulative release of BBR at different time points (W_t) was compared to the total amount of BBR loaded in the nerve conduit (W_0).

2.3 Preparation and characterisation of L-ZBZPGM

A 3% w/v zein solution was prepared by dissolving it in 80% ethanol, followed by the addition of MT at concentrations of 10, 20, and 40 μmol, and stirred for 1 hour at room temperature. Pec was dissolved in a 6% w/v solution of 2% CaCl$_2$, followed by the addition of GO at concentrations of 0, 0.4, 0.8, 1.2, and 1.6 mg mL^{-1}. The mixture was then stirred continuously for four hours at 40 °C. The liquid–liquid dispersion method was employed to incrementally incorporate maize based on the mass ratios of Zein : Pec = 3 : 1, 2 : 1, 1 : 1, 1 : 2, and 1 : 3. The alcohol-soluble protein solution was stirred to create a uniform Zein/Pec/GO/MT (ZPGM) hydrogel precursor. The sol was introduced into the prepared hollow nerve conduit and gelled at room temperature to form a hydrogel composite nerve conduit, which was subsequently freeze-dried at −80 °C to produce the final product. Hydrogels were categorized based on MT concentrations into MT1, MT2, and MT3, the hydrogel group loaded only with the drug is designated as ZPM, and based on GO concentrations into GO0, GO1, GO2, GO3, and GO4. The Zein/Pec/GO hydrogel group was labeled as ZPG, the Zein/Pec/GO/MT hydrogel group as ZPGM, and both the L-Zein/Zein/Pec/GO/MT and L-Zein/Pec/GO/MT groups were designated as L-ZZPGM. The L-Zein/Zein/Pec/GO/MT hydrogel group is set to L-ZPGM.

The hydrogels prepared at different mass ratios were lyophilized and observed by SEM.

The porosity of the hydrogels was determined by gravimetric analysis.[43] All experiments were conducted in triplicate. Hydrogel aerogels with a V_0 rating and regular shape were submerged in hermetically sealed containers containing ethanol. The process was monitored until no further bubbles emerged in the samples, at which point immersion was considered complete. The weight of ethanol within the aerogel pores was determined by the difference between the initial weight (W_0) and the equilibrium weight (W_t). The pore volume (V_p) was determined using the density of ethanol (ρ) with the equation provided.

$$V_p = \frac{(W_t - W_0)}{\rho} \times 100\%$$

The formula for calculating porosity as a percentage was as follows:

$$\text{Porosity}(\%) = \frac{V_p}{V_0} \times 100\%$$

The swelling rate (SR) of the hydrogels was determined using a standard swelling test. The hydrogel was submerged in a phosphate-buffered saline solution (pH 7.4, 37 °C) and periodically weighed (W_t) after removing all external water. The hydrogel was weighed until a state of equilibrium was reached. The SR was determined using the equation:

$$\text{SR}(\%) = \frac{W_t}{W_i} \times 100\%$$

In this context, W_t and W_i represent the initial weights and the weights associated with different swelling times, respectively.

The hydrogel's compressive modulus was measured using a microcomputer-controlled electronic universal testing machine. Hydrogels measuring 20 mm in diameter and 10 mm in thickness were compressed at room temperature using a 10 N load cell at a consistent strain rate of 1 mm min^{-1}.

The degradation properties, drug loading and drug release rate of the hydrogels were consistent with the characterization of the nerve catheters described above.

The conductivity of the hydrogels with different contents of GO was determined by a four-probe resistivity tester, and the hydrogels were co-cultured with RSC96 cells for 2 days. The hydrogels were incubated with CCK-8 and protected from light, and the OD values of the wells were measured by an enzyme marker.

2.4 Cytotoxicity and anti-inflammatory experiments on nerve conduits

Raw264.7 mouse monocyte macrophages and RSC96 rat cells were cultured in DMEM with 10% fetal bovine serum and 1% penicillin/streptomycin.

RSC96 cells were trypsinized to reach a concentration of 1×10^5 cells per mL and cultured in 96-well plates with L-ZB

neurotubule releases on days 7, 14, and 21, adding 100 μL of cell suspension per well. Following a five-day period of cultivation, the viability of the cells was assessed through the utilisation of a CCK-8 assay and fluorescence microscopy (IX71, Olympus, Japan). Prior to observation, the cells were labelled with Calcein-AM Istaining for a period of 15 minutes.

Lipopolysaccharide (LPS) was typically employed to simulate the impact of inflammation on cellular processes. RAW264.7 cells were cultured in 96-well plates for 24 hours to facilitate adherence, and subsequently divided into four groups. The latter three groups were then replaced with cell culture medium containing 1 mg mL^{-1} LPS, creating a blank control group, LPS group, L-Zein group and L-ZB group. These were then cultured in a cell culture incubator for 2 days. After this period, cell activity was detected using a NO assay kit. The remaining parallel groups were fixed with 4% paraformaldehyde for a period of 30 minutes. Cell membranes were stained with 1,1′-dioctadecyl-3,3′,3′-tetramethylindocarbocyanine perchlorate (DiI), and nuclei with 4′,6-diamidino-2-phenylindole (DAPI) for 30 minutes. Subsequently, the Raw264.7 cells that had been immobilized on the material were observed under a fluorescence inverted microscope.

2.5 Cytotoxicity and antioxidant assay of hydrogel composite nerve conduit

Before the introduction of the cells, the ZPG, ZPGM, L-ZZPGM and L-ZBZPGM groups were subjected to a sterilization process. RSC96 cells were lysed using trypsin, diluted to 1×10^5 cells per mL, and then cultured with the specified materials. Cell viability was evaluated after a five-day culture using a CCK-8 assay and fluorescence microscopy (IX71, Olympus, Japan). Prior to observation, the cells were labelled with Calcein-AM staining for a period of 15 minutes.

A peroxide environment was created for RSC96 cells by configuring 120 μM *tert*-butyl hydroperoxide (TBHP), and mitochondrial levels in live cells were determined using Mito-Tracker Red CMXRos (Invitrogen). RSC96 cells were incubated with 50 nM Mito-tracker probe at 37 °C for 30 minutes. The cell nuclei were stained with the DNA-specific dye DAPI for a period of 15 minutes at 37 °C. After staining, RSC96 cells were washed with PBS and imaged using a confocal microscope.

2.6 Electrical stimulation experiment

RSC96 cells were trypsinized to achieve a concentration of 1×10^5 cells per mL and then applied to the composite nerve conduit surface. The cells were then cultured for 24 hours. After 24 hours, the RSC96 cells were electrically stimulated with different potentials. The optimal voltage and time of electrical stimulation were identified through observation of cell viability using the CCK-8 assay.

The OD values of the various groups following electrical stimulation were determined by CCK-8, and the membranes and nuclei of RSC96 cells were stained with DiI and DAPI. The RSC96 cells on the material were observed under a fluorescence inverted software was utilized for image analysis.

3.   Results and discussion

As shown in Fig. 1, Cys and Zein were subjected to a disulfide exchange reaction, transforming the hydrophobic material into an amphoteric one. Electrospinning was performed on an iron rod with a diameter of 2 mm. After removing the iron rod, a hollow nerve conduit loaded with BBR was fabricated, thereby endowing it with anti-inflammatory properties. Subsequently, a hydrogel was synthesized *via* chemical cross-linking between the $-NH_2$ groups of Zein and the $-COOH$ groups of Pec. This hydrogel, enriched with MT and GO, was formulated into a conductive material with antioxidant capabilities. Upon injection into the nerve conduit, the resultant entity, L-ZBZPGM, which demonstrated both anti-inflammatory and antioxidant attributes.

3.1   Characterization of nerve conduits

As illustrated in Fig. 2(A), Zein displayed absorption peaks in the range of $3200-3400$ cm^{-1}, suggesting the presence of an N–H stretched vibration and hydrogen bonding within the system, as marked by the Amide A band. The peak at 3284 cm^{-1} signifies the hydrophilic O–H stretching of the protein, while the vibration at 2956 cm^{-1} denotes hydrophobic C–H bending within the protein. After modification with Zein, Cys displayed absorption peaks at 1296, 1058 and 859 cm^{-1} within the fingerprint region. The peaks at 3284 cm^{-1} and 2956 cm^{-1} represented the hydrophilic O–H and hydrophobic C–H protein stretching, respectively. Upon modification with Zein, the fingerprint region of Cys retained absorption peaks at 1296, 1058, and 859 cm^{-1}. It was observed that the magnitude of the hydrophilic O–H stretching increased, while the hydrophobic C–H stretching decreased. This outcome confirmed the successful preparation of L-Zein.

The finalized electrostatically spun wire was presented in Fig. 2(B) as a hollow nerve conduit.

The SEM images of Zein and L-Zein, depicted in Fig. 2(C) and (D), reveal the formation of smooth nanofibers on the collector with diameters of 2.35 ± 0.85 μm for Zein fibers and 3.61 ± 1.19 μm for L-Zein fibers. Notably, there was minimal variation in the diameter range before and after modification, indicating that the Cys modification of Zein exerted no significant impact.

Existing literature robustly demonstrates that amphoteric materials promote cell adhesion, whereas both hydrophobic and excessively hydrophilic materials impede it.[44] As illustrated in Fig. 2(E), the water contact angle of the Zein group was 110°, indicative of its hydrophobic nature. In contrast, Fig. 2(F) revealed that the water contact angle for L-Zein had decreased to 92°, suggesting enhanced hydrophobicity. This enhancement can be attributed to the Cys-induced modification of the
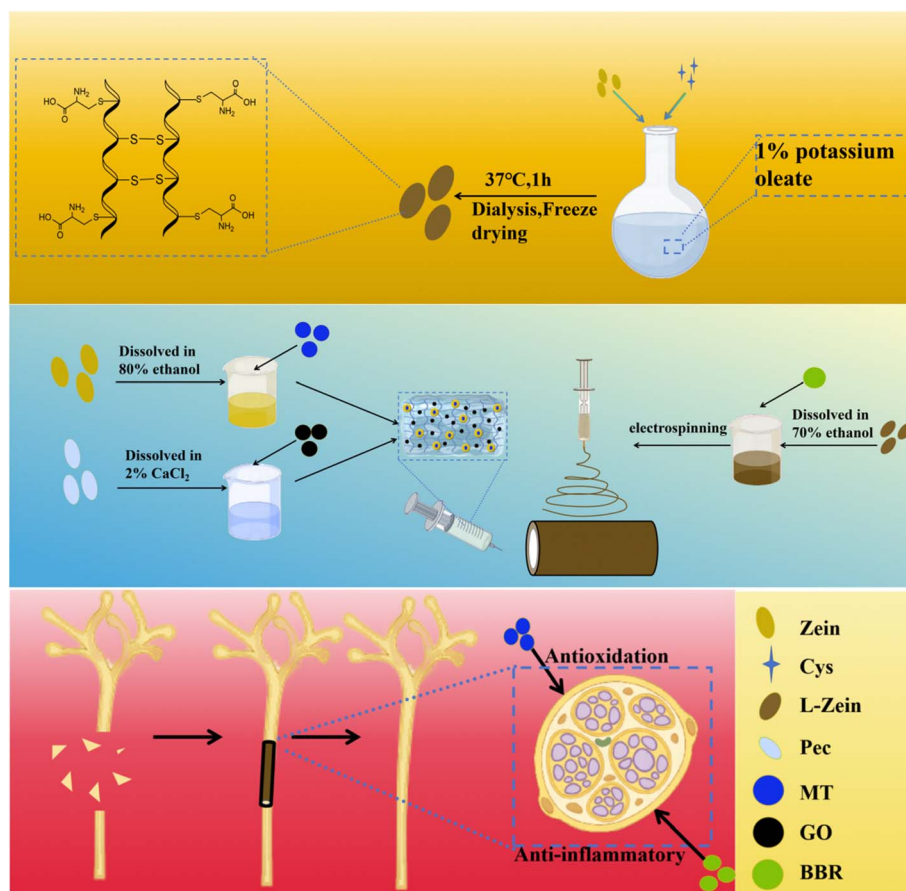

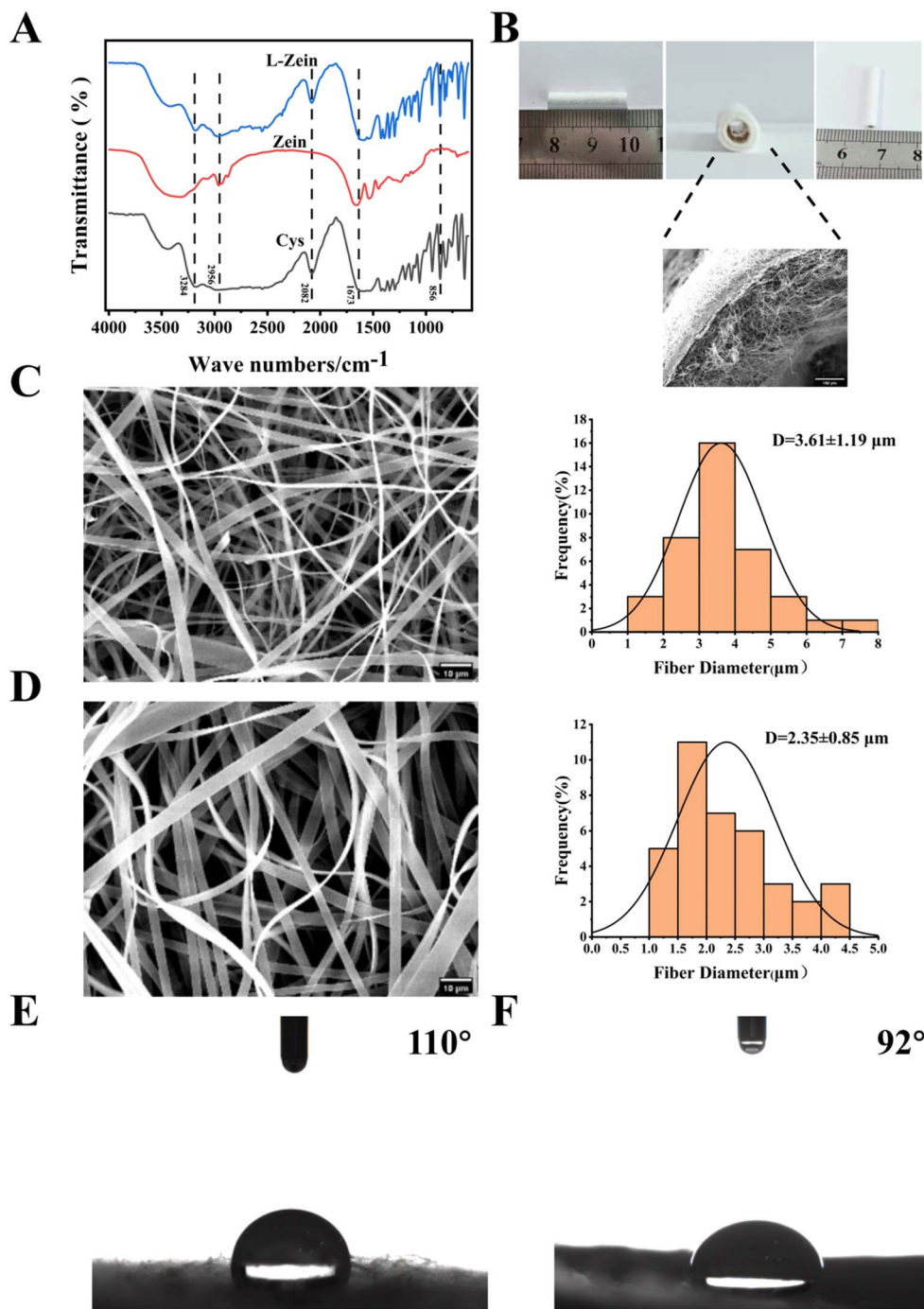Fig. 1   Flowchart of L-ZBZPGM preparation process.

Fig. 2 (A) FTIR spectra of Cys, Zein, and L-Zein. (B) L-Zein nerve conduit. (C) SEM image and diameter distribution of Zein (scale bar = 10 μm). (D) SEM image and diameter distribution of L-Zein (scale bar = 10 μm). (E) Water contact angle map of Zein. (F) Water contact angle map of L-Zein.

protein, characterized by the disruption and subsequent reorganization of disulfide bonds, thereby altering the spatial structure of Zein.

The hydrogel used for nerve regeneration must maintain suitable mechanical properties to ensure structural integrity and resist forces from surrounding tissues. These properties are typically assessed by evaluating the tensile strength of the nerve conduits.[45–47] The measured tensile strengths of Zein and L-Zein catheters were 3.42 ± 0.43 MPa and 3.22 ± 0.35 MPa,

respectively. These results reveal no significant difference between the two, and both materials meet the mechanical requirements for nerve repair as demonstrated in Fig. 3(A). Furthermore, the mechanical properties of the nerve catheter remained largely consistent following Cys modification.

The residual mass ratios of the Zein catheter and L-Zein catheter, post-two weeks, were found to be $32.52 \pm 2.43\%$ and $26.78 \pm 1.95\%$ respectively, with a significant difference (*$p <$ 0.05), as shown in Fig. 3(B). This can be attributed to the
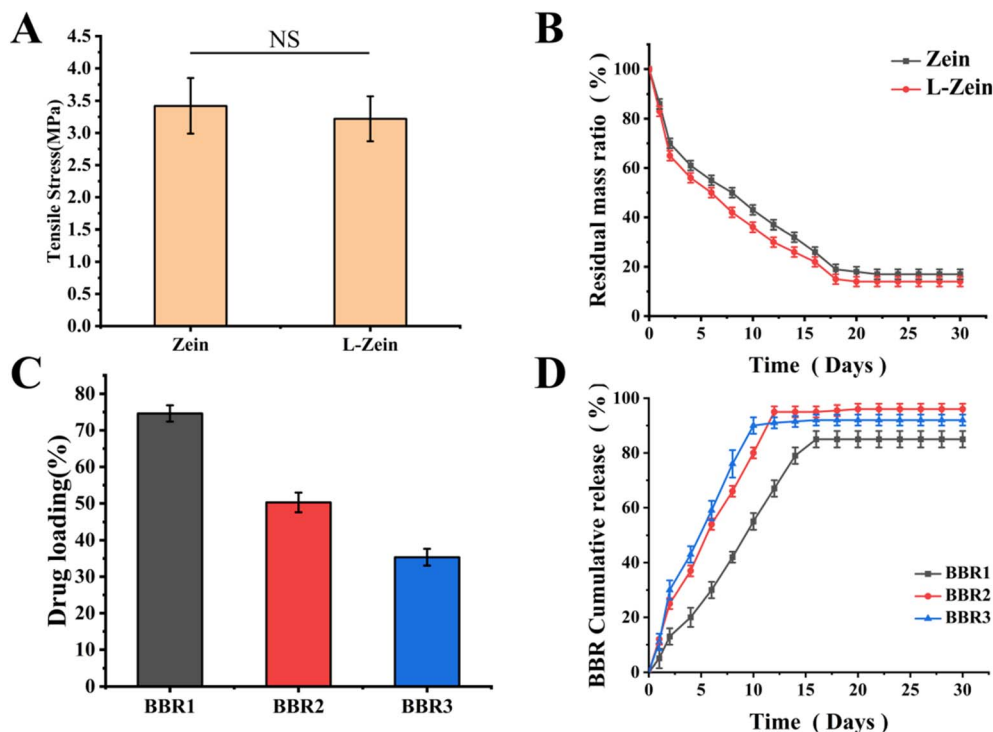
Fig. 3 (A) Tensile strength of Zein and L–Zein nerve conduits. (B) Degradation of Zein and L–Zein nerve conduits. (C) Drug loading of nerve conduits with different BBR concentrations. (D) Cumulative release rate of nerve conduits with different BBR concentrations.

increased hydrophilicity and ease of degradation of the modified L-Zein, resulting from alterations in its spatial structure.

Research has demonstrated that BBR at a concentration of 5 μmol possesses anti-inflammatory properties in β-amyloid-treated cells, primarily through the inhibition of the production and release of inflammatory cytokines.[48] As the catheter was placed in PBS containing lysozyme, the catheter gradually degraded, its spatial structure changed, and BBR was gradually released. As shown in Fig. 3(C) and (D), the drug loading efficiency for theBBR1 group was $74.62 \pm 2.23\%$, with peak release observed on the 16th day. The release rate stood at $85.31 \pm 2.16\%$. For the BBR2 group, the drug loading efficiency was $50.25 \pm 2.69\%$, with its peak release occurring on the 14th day and are lease rate of $96.31 \pm 2.44\%$. The BBR3 group had a drug loading efficiency of $35.33 \pm 2.31\%$ and reached its peak release on the 10th day, showcasing a release rate of $92.38 \pm 2.03\%$. The diminished loading efficiency in the BBR3 group can be attributed to the high concentration of BBR, where the majority remains in a free state, with only a smaller portion being encapsulated within the catheter. Given the results, the BBR2 group, which exhibited drug loading and release parameters closest to 5 μmol, was chosen for subsequent experiments.

3.2   Characterisations of L-ZBZPGM

Fig. 4 illustrated the morphology of hydrogels at varying mass ratios of Zein/Pec, as visualized through SEM. All observed hydrogels displayed a continuous network structure. Fig. 4(A) and (B) suggest that the network structure created by these gels

was relatively looser, with pore sizes measuring 183.02 ± 59.47 μm and 202.58 ± 64.50 μm for Zein : Pec ratios of 3 : 1 and 2 : 1 respectively. This is attributed to the smaller proportion of Pec and reduced physical cross-linking. Fig. 4(C) and (D) illustrate hydrogel pore diameters of 174.33 ± 36.27 μm and 166.54 ± 36.01 μm when the Zein : Pec ratio is 1 : 1 and 1 : 2 respectively, showcasing a tightly and neatly arranged pore structure.

Research has demonstrated that a larger porosity (>75%) enhances substance exchange within the tissue and promotes peripheral nerve regeneration. However, an excessively high pore gland ratio (>95%) is not ideal, as it hinders the loading of drugs into the hydrogels due to rapid dissolution in the solution.[49] In this study, Zein contains numerous $-NH_2$ groups, while Pec contains many $-COOH$ groups. Ionic bonds are formed between $-NH_2$ and $-COOH$. Pec, when dissolved in $CaCl_2$, forms physical cross-links with calcium ions. This ultimately results in a hydrogel with both chemical and physical cross-linking. GO, which contains a large number of $-COOH$ groups, forms hydrogen bonds with the hydrogel and undergoes physical adsorption and encapsulation. The hydrogel is then loaded with MT and GO to form the ZPGM hydrogel. Fig. 5(A) showed the morphological images of L-ZBZPGM. Fig. 5(B) illustrates significant changes in pore size in hydrogels with varying mixing ratios. As the Zein/Pec ratio shifted from 3 : 1 to 1 : 3, there was a consistent decrease in porosity. This can be attributed to the increasing dominance of physical cross-linking over chemical cross-linking as Pec content increases, with the former exhibiting greater strength. The porosity measured $76.73 \pm 3.51\%$ and $74.24 \pm 2.43\%$ when the Zein/Pec
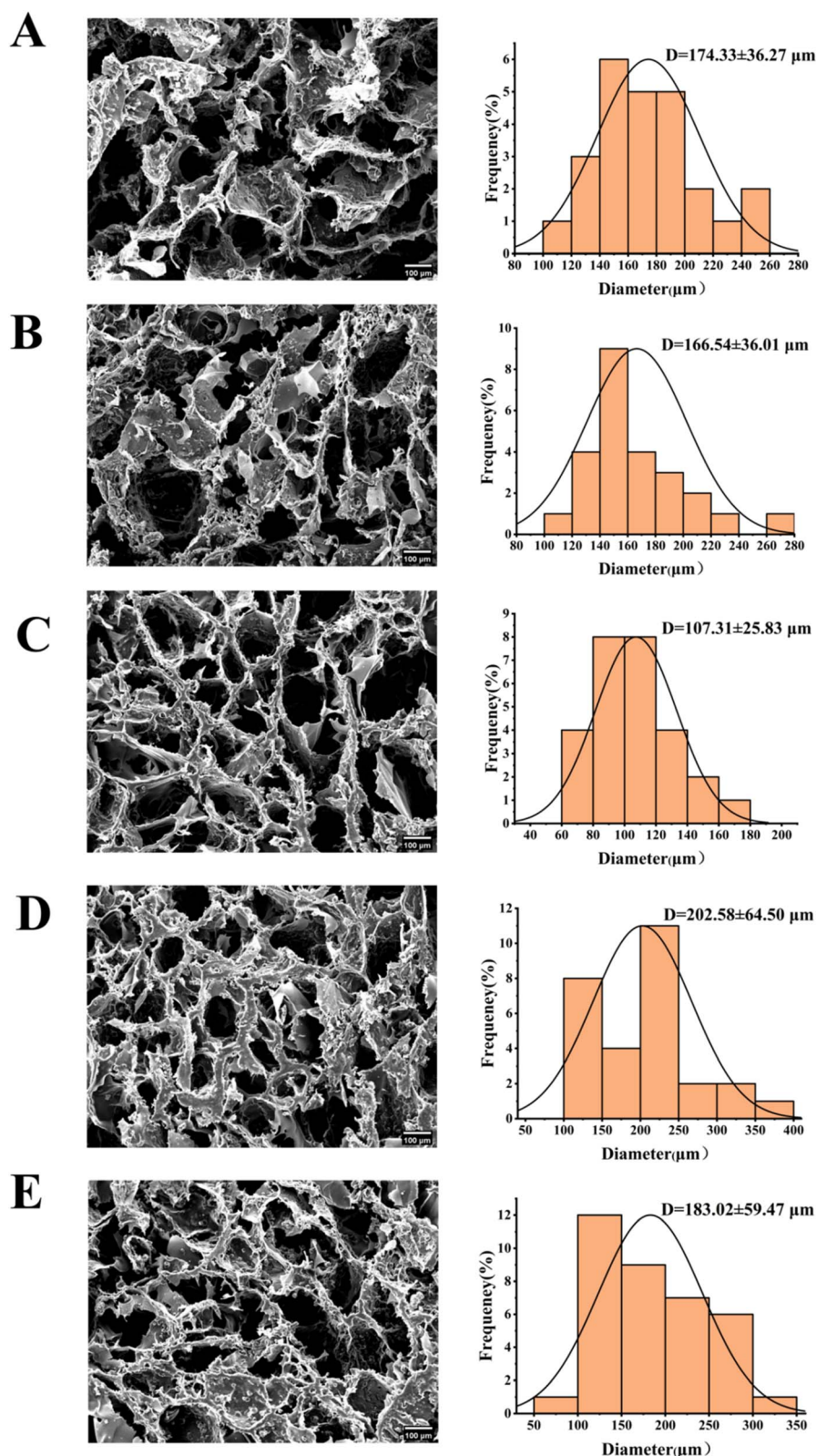
Fig. 4 (A) Scanning electron microscopy and pore size distribution of the hydrogel with Zein : Pec = 3 : 1. (B) Scanning electron microscopy and pore size distribution of the hydrogel with Zein : Pec = 2 : 1. (C) Scanning electron microscopy and pore size distribution of the hydrogel with Zein : Pec = 1 : 1. (D) Scanning electron microscopy and pore size distribution of the hydrogel with Zein : Pec = 1 : 2. (E) Scanning electron microscopy and pore size distribution of the hydrogel with Zein : Pec = 1 : 3.
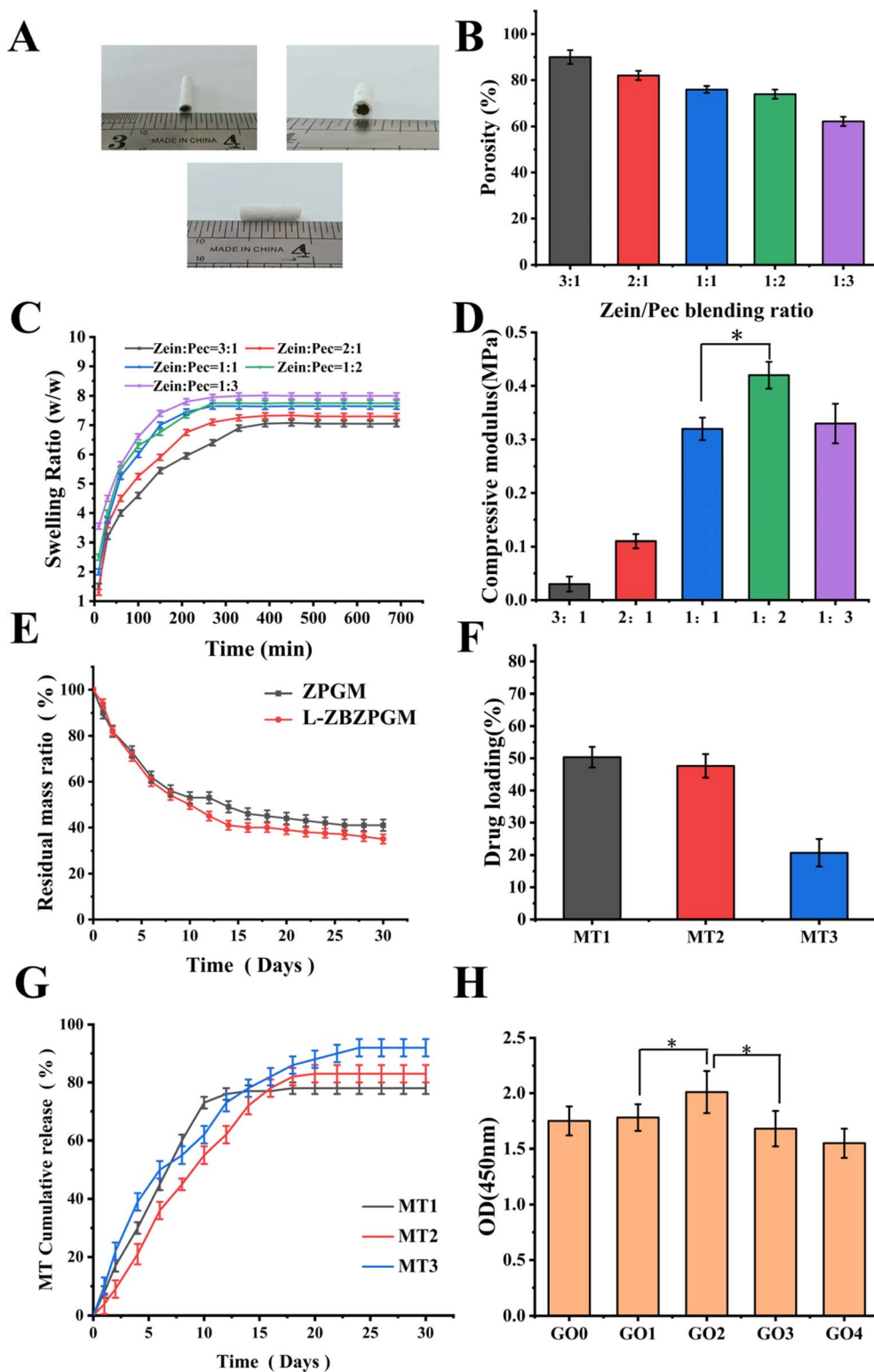
Fig. 5 (A) Morphological images of L-ZBZPGM. (B) Porosity of Zein/Pec hydrogels at different ratios. (C) Swelling rate of Zein/Pec hydrogels at different ratios. (D) Compression modulus of Zein/Pec hydrogels at different ratios (*$p < 0.05$). (E) Degradation of ZPGM and L-ZBZPGM. (F) Loadings of hydrogels at different concentrations of MT (ZPM). (G) Cumulative release rate of hydrogels at different MT (ZPM). (H) OD values of RSC96 cells at different concentrations of GO (*$p < 0.05$) (ZPG).

ratio was $1 : 1$ and $1 : 2$ respectively, showing negligible differences in results.

Fig. 5(C) illustrated the swelling behavior of various hydrogels. As the Zein/Pec ratio transitioned $3 : 1$ to $1 : 3$, the swelling rate declined from 8.01 ± 0.25 to 7.05 ± 0.44. With Zein/Pec ratios of $1 : 1$ and $1 : 2$, the corresponding swelling rates were 7.64 ± 0.39 and 7.75 ± 0.25, respectively—suggesting that these rates do not significantly differ. This implies that the porosity and swelling rate of hydrogels remain relatively consistent, regardless of the Zein/Pec ratio, be it $1 : 1$ or $1 : 2$. The results indicate that both ratios yield similar porosity and swelling rates, both of which are suitable for nerve repair.

For optimal performance, the nerve regeneration hydrogel must possess suitable mechanical properties to maintain its structural integrity and resist stress from surrounding tissues. Fig. 5(D) illustrates the stress–strain curves of assorted hydrogels. The Zein/Pec hydrogel, at a ratio of $1 : 2$, demonstrated a compressive modulus of 0.42 ± 0.025 MPa. This was notably greater than the 0.32 ± 0.021 MPa recorded for the $1 : 1$ ratio. Owing to its superior porosity, solubility, and compressive strength, the $1 : 2$ ratio was chosen for subsequent experiments.

As shown in Fig. 5(E), the degradation process of the ZPGM group was attenuated due to the integration of GO,[29] with a resultant residual mass ratio of $49.23 \pm 2.52\%$ after a period of two weeks. The residual mass ratio of the L-ZBZPGM group at the end of the 30 days degradation period was $35.15\% \pm 1.87\%$, which was significantly different from that of the ZPGM group (*$p < 0.05$), thereby satisfying the prerequisites for nerve repair.

Existing literature suggests that MT at a concentration of 10 μmol enhances Parkin expression in RSC96 cells via melatonin, stimulates mitochondrial autophagy, and impedes apoptosis. However, cell viability begins to deteriorate upon reaching an MT concentration of 20 μmol.[37] As the hydrogel was placed in PBS containing lysozyme, the hydrogel gradually degraded, its spatial structure changed, and MT was gradually released. As shown in Fig. 5(F) and (G), the drug loading rates for groups MT1, MT2, and MT3 were found to be $50.33 \pm 3.21\%$, $47.63 \pm 2.56\%$, and $20.67 \pm 4.23\%$ respectively. Peak release occurred on the 12th day for MT1, with a rate of $78.28 \pm 2.03\%$, on the 18th day for MT2, with a rate of $83.31 \pm 3.64\%$, and on the 24th day for MT3, with a rate of $92.38 \pm 2.83\%$. Notably, the drug loading and release profile of the MT2 group closely mirrored that of 10 μmol, thus it was selected for subsequent experiments.

Conductivity was a pivotal factor in evaluating the effectiveness of conductive hydrogels. Optimal conductivity not only mimicked the unique electrical microenvironment of neural tissues but also enhanced the adhesion, migration, proliferation, and differentiation of electrically active cells via electrical stimulation. As illustrated in Table 1, a higher GO content led to a corresponding increase in hydrogel conductivity, with values surpassing 10^{-4} S cm^{-1}. Such conductivity was sufficient to foster the beneficial effects of electrical stimulation on nerve tissue regeneration.

Fig. 5(H) presents the cellular optical density (OD) values of RSC96 cells after electrical stimulation. As the GO content escalated from 0.4 mg mL^{-1} to 1.6 mg mL^{-1}, the OD values were recorded as 1.78 ± 0.12, 2.01 ± 0.19, 1.68 ± 0.16, and 1.55 ± 0.13, respectively. These results suggest an initial increase, followed by a decrease, with the peak OD value observed at 0.8 mg mL^{-1}. A significant difference (*$p < 0.05$) was noted, indicating that the highest cellular activity occurred at this concentration.

To conclude, the ultimate concentration of GO within the synthesized ZPGM hydrogel was measured to be 0.8 mg mLl^{-1}.

3.3 Cytotoxic and anti-inflammatory characterization of nerve conduits

To evaluate the impact of the L-Zein/BBR nerve conduit on cell proliferation, RSC96 cells were cultured for five days. Subsequently, the conduit was introduced on days 7, 14, and 21. Cells cultured under standard conditions served as the control, while cells treated with 1 μM BBR acted as a negative control. Cell activity was determined using Calcein-AM and CCK-8 assays. Following staining, live cells emitted green fluorescence, evident in Fig. 6(A). These cells exhibited a healthy morphology, suggesting their viability, a finding corroborated by the CCK-8 assay data. As illustrated in Fig. 6(B), the OD values for all groups increased on days 3 and 5, with a significant difference (*$p < 0.05$), highlighting the significant proliferative activity of the BBR-loaded nerve conduit. Among the time points tested, the 21 days release solution showed the most pronounced proliferative effect, followed by the 14 days and 7 days solutions. This can be attributed to the increased BBR concentration in the solution over extended release periods, which in turn enhanced RSC96 cell proliferation.

The diminished cell count and elevated NO content in the LPS group suggest that the cells are influenced by inflammatory factors, exhibiting the lowest cell activity. As shown in Fig. 7(A) and (B), DiI stains the RSC96 cell membrane red, while DAPI stains the nucleus blue. In the control group, the cells had evolved from their initial round shape to a spindle form, exhibiting multiple axons. However, the cells in the L-Zein group were deficient in BBR, leading to increased NO levels and diminished cellular activity. Compared to the LPS group, the L-ZB group exhibited elevated cellular activity, characterized by a notable increase in cell number and a marked reduction in NO content, with a significant difference (**$p < 0.01$). These observations indicate that BBR-containing neural conduits exhibit anti-inflammatory properties. Furthermore, the L-ZBZPGM group demonstrated that MT potentially synergized with BBR, leading to a heightened anti-inflammatory effect.

Table 1 Electrical conductivity of Zein/Pec hydrogels at different concentrations of GO

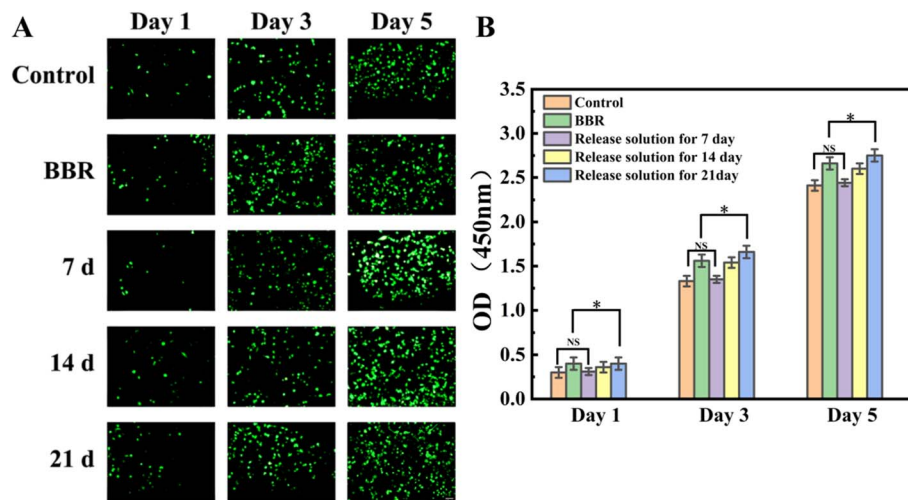| Samples	Zein/Pec	Zein/Pec/GO1	Zein/Pec/GO2	Zein/Pec/GO3	Zein/Pec/GO4
Conductivity (10^{-3} s cm^{-1})	0	0.69 ± 0.265	1.23 ± 0.482	1.47 ± 0.294	1.61 ± 0.371

Fig. 6 (A) Live cell staining of RSC96 cells in L–Zein/BBR nerve conduit extraction solution on days 1, 3, and 5 (scale bar = 10 μm). (B) OD values of RSC96 cells in L–Zein/BBR nerve conduit extraction solution on days 1, 3, and 5 (*p < 0.05).
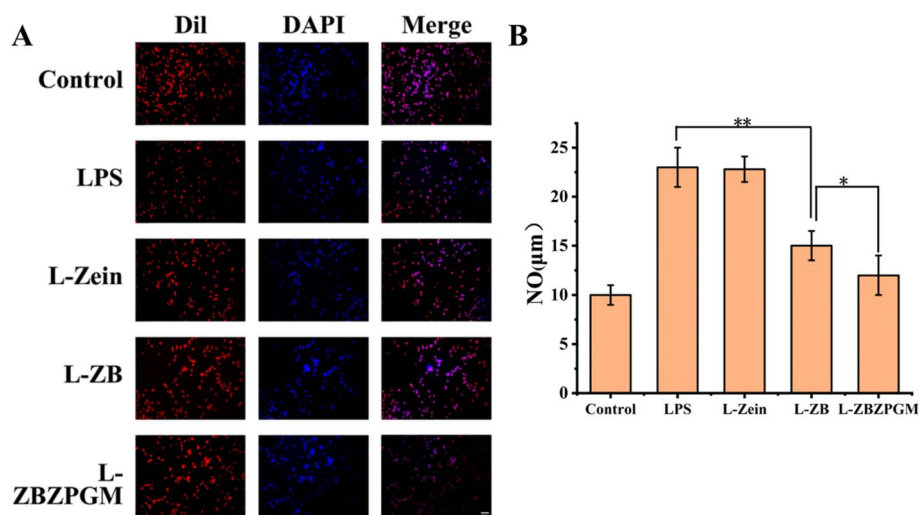

Fig. 7 (A) Fluorescent staining of RSC96 cells following treatment with different materials (scale bar = 10 μm). (B) NO concentration in RSC96 cells post-treatment with various materials (*p < 0.05, **p < 0.01).

3.4 Cytotoxicity and antioxidant characterization of hydrogel composite nerve conduits

To evaluate the influence of hydrogel composite nerve conduits on cell proliferation, RSC96 cells were cultured on nerve conduits infused with ZPG hydrogel, both with and without the addition of BBR and MT. Normally cultured cells were used as a negative control. As illustrated in Fig. 8(A) and (B), the optical density (OD) values of the experimental groups displayed considerable similarity on the first day of the culture period, with no statistically significant differences. The OD values for each experimental group increased on days 3 and 5, with a significant difference (*p < 0.05), demonstrating the hydrogel's robust proliferative activity. The OD values for the ZPG hydrogel were not significantly different from those of the control group, suggesting non-cytotoxicity. Conversely, the ZPGM hydrogel displayed significantly elevated OD values,

indicative of effective MT release and sustained biological activity. Furthermore, the L-ZBZPGM group exhibited significantly higher OD values than the control group on all days (**p < 0.01), signifying enhanced cell proliferation due to the hydrogel composite nerve conduit. The calcium xanthophyll AM fluorescence staining of RSC96 cells aligned with the findings of the CCK8 assay.

To evaluate the antioxidant properties of the hydrogel composite nerve conduit, TBHP was employed to simulate a peroxidative environment in RSC96 cells, thereby affecting mitochondrial function and overall cellular growth. Mito-tra, a prevalent mitochondrial stain, interacts with active mitochondria, emitting red fluorescence. The intensity of this fluorescence is directly proportional to cellular activity. As shown in Fig. 9(A) and (B), there was a notable reduction in the red fluorescence intensity of Mito-tra when TBHP was introduced,
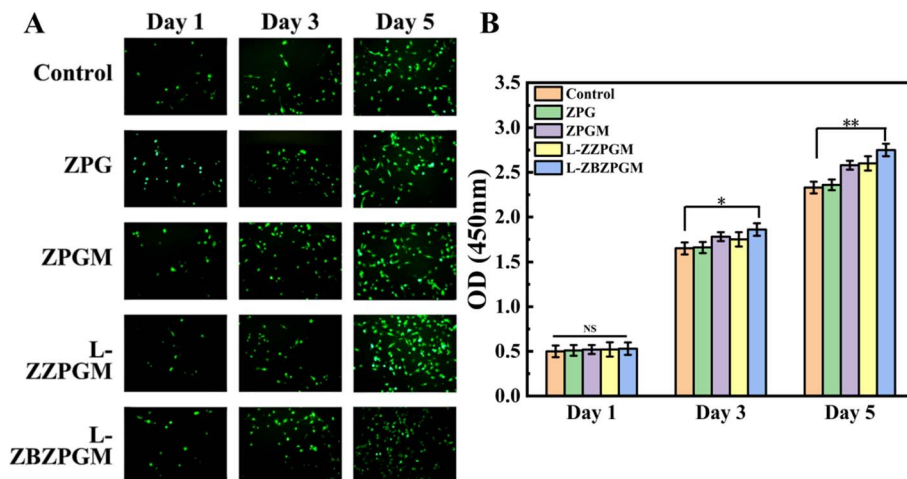
Fig. 8 (A) Live cell staining plots of hydrogel composite nerve conduit immersion solution after days 1, 3 and 5 of culturing RSC96 cells (scale bar = 10 μm). (B) OD values of hydrogel composite nerve conduit extraction solution after culturing RSC96 cells on days 1, 3 and 5 (*$p < 0.05$, **$p < 0.01$).
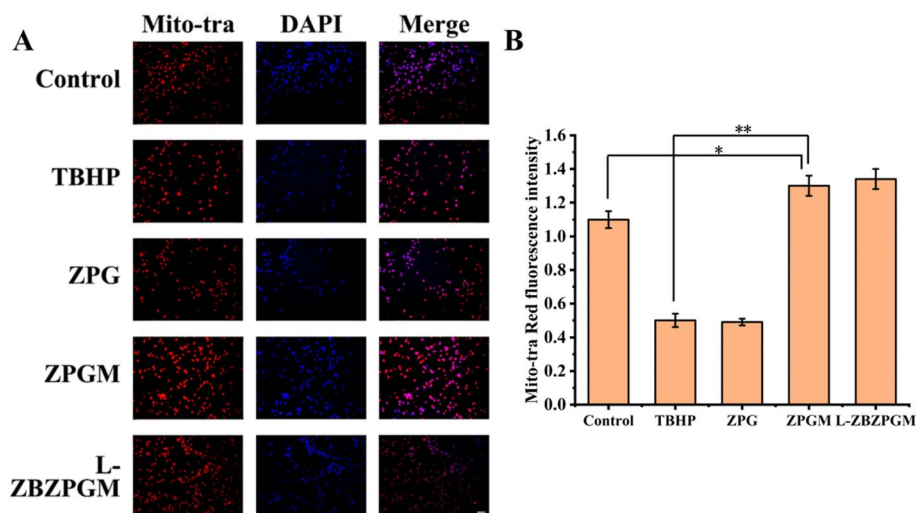

Fig. 9 (A) Fluorescence staining of mito-tra and DAPI in RSC96 cells post-treatment with different materials (scale bar = 10 μm). (B) mito-tra red fluorescence intensity following treatment with various materials (*$p < 0.05$, **$p < 0.01$).

in comparison to the control, thereby validating the model. The fluorescence intensity in the ZPG group was comparable to that of the TBHP group due to the lack of MT. However, upon adding MT, the fluorescence intensity in the ZPG group significantly surpassed that of the control (*$p < 0.05$), highlighting the antioxidant attributes of MT and its beneficial effect on celluar growth. Notably, the ZBZPGM group exhibited the highest fluorescence intensity, suggesting a synergistic effect between MT and BBR (**$p < 0.01$), which is more conducive to cell proliferation.

3.5 Electrical stimulation experiment

As shown in Fig. 10(A) and (B), there is a direct correlation between increased voltage of electrical stimulation and the OD value of the cells; as the voltage increases, so does the OD value.

This increase is more pronounced within the 100 mV range. However, it was observed that as the voltage continued to rise in later stages, the growth rate of the cell's OD value decelerated. The study also examined the impact of the duration of external electrical stimulation on cell proliferation under a fixed stimulation voltage. It was found that the highest OD value indicating optimal cell growth conditions was achieved when the electrical stimulation was set at 36 h. In conclusion, for subsequent electrical stimulation experiments, the selected parameters were a stimulation voltage of 250 mV and a stimulation duration of 36 h.

Fig. 10(C) depicts the fluorescence staining graphs of RSC96 cells, while Fig. 10(D) illustrates the OD measurements of RSC96 cells post electrical stimulation. These graphs suggest that external electrical stimulation does not significantly
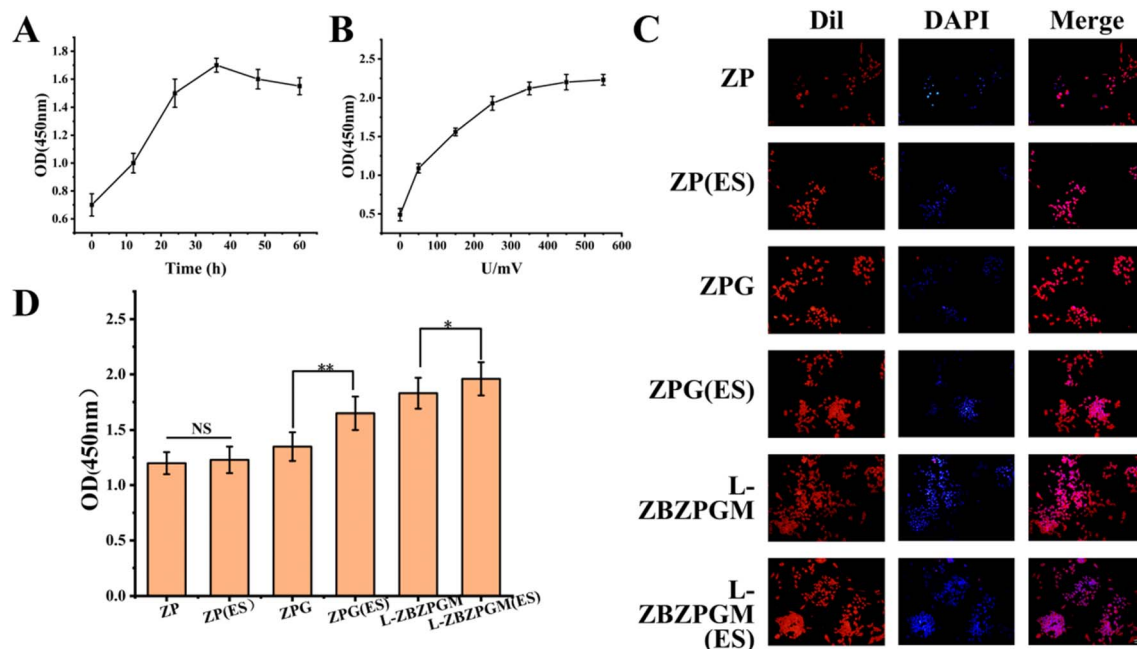
Fig. 10 (A) OD values of RSC96 cells following stimulation at varying voltages. (B) OD values of RSC96 cells following varying duration of electrical stimulation. (C) Fluorescent staining of RSC96 cells following electrical stimulation experiments (scale bar = 10 μm). (D) OD values of RSC96 cells post-electrical stimulation ($*p < 0.05$, $**p < 0.01$).

influence cell growth in both the ZP hydrogel and ZP (ES) hydrogel groups. This is largely due to the absence of conductive substances which prevents direct microcurrent stimulation through the medium liquid. However, once GO is incorporated into the hydrogel, the material exhibits conductivity, enabling it to mediate electric current and thus stimulating the cells adhered to it. Cells in the ZPG (ES) group predominantly exhibited a shuttle structure with evident axons, signifying clear cell differentiation. The quantity of these cells was large and they were densely spread. On the other hand, the ZPG group had fewer cells with a more rounded morphology and limited axon growth compared to the ZPG (ES) group. Interestingly, the L-ZBZPGM (ES) group displayed dense cell growth with extensive axon development forming a network. In comparison, the L-ZBZPGM group, while having fewer cells, still demonstrated good growth with some presence of axons. The L-ZBZPGM group exhibited a small number of cells with satisfactory growth, and some cells developed axons. A comparative analysis of cell numbers and axon presence suggests that the addition of GO to the hydrogel allows it to conduct microcurrent, generating electric stimulation for the adhered cells. This consequently promotes cell proliferation, differentiation, and growth to a certain degree.

4. Conclusion

L-ZBZPGM exhibited superior mechanical properties and degradation characteristics, with its three-dimensional structure ensuring the sustained release of BBR and MT. Fluorescence staining of RSC96 cells demonstrated that Zein modified with Cys was more conducive to cell growth. The LPS test using

Raw264.7 cells proved that the nerve conduit loaded with BBR had significant anti-inflammatory effects. The use of RSC96 cells with TBHP to simulate peroxide environment showed that the hydrogel loaded with MT had antioxidant properties. Moreover, the incorporation of conductive GO combined with electrical stimulation could induce rapid proliferation of RSC96 cells, indicating that L-ZBZPGM could enhance nerve regeneration under electrical stimulation. BBR served to mitigate the impact of inflammatory factors on cells, while MT enhances mitochondrial activity to combat peroxidative factors. Together, they exerted synergistic effects to promote nerve regeneration.

This study has confirmed that L-ZBZPGM can overcome the limitations of single nerve conduit repair, making it an ideal drug delivery carrier and a promising material for applications. Despite the great potential shown by hydrogel composite nerve conduits, further research is needed to comprehensively understand their degradation and drug release rates within the body. Additionally, the impact of excess energy on cells during electrical stimulation also warrants in-depth investigation. We plan to conduct animal experiments next to further explore the degradation and nerve repair effects of L-ZBZPGM *in vivo*.

Author contributions

Runtian Xu: conceptualization, methodology, validation, formal analysis, writing – original draft. Hanping He: conceptualization, methodology, validation. Huan Deng: supervision, draft revision. Yuehan Dong: methodology, data curation, investigation. Xiangjie Wu: investigation. Zinuo Xia: software, investigation. Yang Zhou: software, investigation. Lin Yang: investigation. Zhijun Huang: resources. Wenjin Xu:

supervision, review of the draft. Peihu Xu: conceptualization, funding acquisition, resources, supervision, review of the draft. Haixing Xu: conceptualization, funding acquisition, resources, supervision, review of the draft.

Conflicts of interest

The authors declare that they have no known competing financial interests or personal relationships that could have appeared to influence the work reported in this paper.

Acknowledgements

References

1 S. Karimi, Z. Bagher, N. Najmoddin, S. Simorgh and M. Pezeshki-Modaress, Alginate-magnetic short nanofibers 3D composite hydrogel enhances the encapsulated human olfactory mucosa stem cells bioactivity for potential nerve regeneration application, *Int. J. Biol. Macromol.*, 2020, **167**(15), 796–806.

2 E. L. Errante, T. Smartz, M. C. Costello, E. A. Schaeffer, A. J. Kloehn, J. Yunga Tigre, *et al.*, Assessing survival, distribution, and optimal loading technique of schwann cell–derived exosomes into second-generation axon guidance channels, *Mil. Med.*, 2024, **19**, 63–66.

3 T. Lu, W. Peng, Y. Liang, M. Li, D.-S. Li, K.-H. Du, J.-H. Wu, *et al.*, PTEN-silencing combined with ChABC-overexpression in adipose-derived stem cells promotes functional recovery of spinal cord injury in rats, *Biochem. Biophys. Res. Commun.*, 2020, **532**(3), 420–426.

4 M. Dong, Q. Xiao, J. Hu, X. Li, D. Guo and B. J. Wang, Meningeal melanocytoma in the cerebellopontine angle: a rare case report and review of the literature, *Oncol. Transl. Med.*, 2021, **7**(1), 35–40.

5 Y. Li, J. Huang, Y. Chen, S. Zhu, Z. Huang, L. Yang, *et al.*, Nerve function restoration following targeted muscle reinnervation after varying delayed periods, *Neural Regener. Res.*, 2023, **18**(12), 2762–2766.

6 S. Rochkind, M. Almog and Z. Nevo, Reviving matrix for nerve reconstruction in rat model of acute and chronic complete spinal cord injury, *Neurol. Res.*, 2022, **12**, 1132–1141.

7 M. Balamurugan, K. Ponnaiah Sathish, L. Daeho and L. Sungwon, Multichannel carbon nanofibers: pioneering the future of energy storage, *ACS Nano*, 2024, **18**(40), 27287–27316.

8 X. Wang, R. Zhao, J. Wang, X. Li, L. Jin, W. Liu, *et al.*, 3D-printed tissue repair patch combining mechanical support

9 R. Xiang, J. Chen, J. Dang, H. Zhu, Z. Ran, Y. Dong, *et al.*, Electrospun silk fibroin/polylactic acid conduit filled with proangiogenic carboxylated silk fibroin/chitosan hydrogel facilitates peripheral nerve regeneration, *Int. J. Polym. Mater. Polym. Biomater.*, 2024, **14**(37), 233–8138.

10 D. Farhan, M. Mojdeh, J. Alireza, K. Mehran and N. Najmeh, Piezoelectric bilayer fibrous conduit with gellan/curcumin encapsulated alginate infilling for promotion of sciatic nerve regeneration in the rat models, *Int. J. Biol. Macromol.*, 2025, **286**, 137–833.

11 H. Javidi, A. Ramazani Saadatabadi, S. K. Sadrnezhaad and N. Najmoddin, Conductive nerve conduit with piezoelectric properties for enhanced PC12 differentiation, *Sci. Rep.*, 2023, **13**(1), 120–124.

12 H. Javidi, A. Ramazani Saadatabadi, S. K. Sadrnezhaad and N. Najmoddin, Preparation and characterization of self-stimuli conductive nerve regeneration conduit using co-electrospun nanofibers filled with gelatin-chitosan hydrogels containing polyaniline-graphene-ZnO nanoparticles, *Int. J. Polym. Mater. Polym. Biomater.*, 2022, **25**, 165–175.

13 R. Dimatteo, N. J. Darling and T. Segura, In situ forming injectable hydrogels for drug delivery and wound repair, *Adv. Drug Deliver Rev.*, 2018, **127**, 167–184.

14 P. Roberta, B. Monica, C. Claudio, C. Valeria, C. Valeria and C. Gianluca, Schiff-base cross-linked hydrogels based on properly synthesized poly(ether urethane)s as potential drug delivery vehicles in the biomedical field: design and characterization, *ACS Omega*, 2024, **9**(46), 45774–45788.

15 Z. Julier, A. J. Park, P. S. Briquez and M. M. Martino, Promoting tissue regeneration by modulating the immune system, *Acta Biomater.*, 2017, **53**, 13–28.

16 R. A. Villarreal-Leal, G. D. Healey and B. Corradetti, Biomimetic immunomodulation strategies for effective tissue repair and restoration, *Adv. Drug Delivery Rev.*, 2021, **179**, 113–913.

17 C. Gökdağ, H. Arkar and Ṣ. Pırıldar, Testing a transdiagnostic model including distal and proximal risk factors for depression and anxiety, *Int. J. Cod. Theory*, 2023, **16**(3), 356–374.

18 C. Annunziata, H. Tommaso, B. Diana, V. Silvia, G. Agnese, C. Donato, *et al.*, Safety of zein nanoparticles on human innate immunity and inflammation, *Int. J. Mol. Sci.*, 2024, **25**(21), 11630.

19 F. Li, Y. Chen, S. Liu, X. Pan, Y. Liu, H. Zhao, *et al.*, The effect of size, dose, and administration route on zein nanoparticle immunogenicity in BALB/c mice, *Int. J. Nanomed.*, 2019, **14**, 9917–9928.

20 R. Chakraborty and S. Roy, Angiotensin-converting enzyme inhibitors from plants: a review of their diversity, modes of action, prospects, and concerns in the management of diabetes-centric complications, *J. Integr. Med.*, 2021, **19**(06), 478–492.

21 J. B. Scharnowski, A. Rodriguez-Uribe, A. K. Pal, T. Wang, M. R. Snowdon, M. Misra, *et al.*, Biocomposites from

thermoplastic postindustrial waste starches filled with mineral fillers for single-use flexible packaging, *Macromol. Mater. Eng.*, 2022, **6**, 307.

22 N. Li, K. Zhang, X. Dong, Y. Xu, Z. Tan, G. Cao, *et al.*, Modification of the structure and function of myofibrillar protein by structurally relevant natural phenolic compounds, *Food Biosci.*, 2023, **53**, 102–676.

23 W. H. Teklehaimanot and M. N. Emmambux, Foaming properties of total zein, total kafirin and pre-gelatinized maize starch blends at alkaline pH, *Food Hydrocolloids*, 2019, **97**, 105–221.

24 H. Motta-Romero, Z. Zhang, A. Tien Nguyen, V. Schlegel and Y. Zhang, Isolation of egg yolk granules as low-cholesterol emulsifying agent in mayonnaise, *J. Food Sci.*, 2017, **82**(7), 1588–1593.

25 H. Shuixian, Z. Yanbing, C. Qin, L. Yitong, L. Lin, A. Muhammad Muntaqeem, *et al.*, Pectin based gels and their advanced application in food: from hydrogel to emulsion gel, *Food Hydrocolloids*, 2024, **160**(3), 110–841.

26 X. Tingting, Y. Ruiwen, L. Liqin, L. Hetong and K. Guoyin, Research progress and application of pectin: a review, *J. Food Sci.*, 2024, **89**(11), 6985–7007.

27 P. Kaushik, E. Priyadarshini, K. Rawat, P. Rajamani and H. B. Bohidar, pH responsive doxorubicin loaded zein nanoparticle crosslinked pectin hydrogel as effective site-specific anticancer substrates, *Int. J. Biol. Macromol.*, 2019, **152**, 1027–1037.

28 P. Ghaffari-Bohlouli, H. Golbaten-Mofrad, N. Najmoddin, V. Goodarzi, A. Shavandi and W.-H. Chen, Reinforced conductive polyester based on itaconic acids, glycerol and polypyrrole with potential for electroconductive tissue restoration, *Synth. Met.*, 2022, **293**, 117–238.

29 X. Chen, C. Liu, Z. Huang, X. Pu, L. Shang, G. Yin, *et al*, Preparation of carboxylic graphene oxide-composited polypyrrole conduits and their effect on sciatic nerve repair under electrical stimulation, *J. Biomed. Mater. Res., Part A*, 2019, **107**(34), 1549–3296.

30 A. Domínguez-Bajo, A. González-Mayorga, C. R. Guerrero, F. J. Palomares, R. García, E. López-Dolado, *et al.*, Myelinated axons and functional blood vessels populate mechanically compliant rGO foams in chronic cervical hemisected rats, *Biomaterials*, 2018, **192**, 461–474.

31 G. Shanshan, N. Hong, J. Lei and C. Qunfeng, Learning from nature: constructing high performance graphene-based nanocomposites, *Mater. Today*, 2016, **20**(4), 1369–7021.

32 N. Golafshan, M. Kharaziha and M. Fathi, Tough and conductive hybrid graphene-PVA: alginate fibrous scaffolds for engineering neural construct, *Carbon*, 2017, **111**, 752–763.

33 H. Amini, A. Rezabakhsh, M. Heidarzadeh, M. Hassanpour, S. Hashemzadeh, *et al.*, An examination of the putative role of melatonin in exosome biogenesis, *Front. Cell Dev. Biol.*, 2021, **9**, 686551.

34 B. Li, X. Cheng, A. Aierken, J. Du, W. He, M. Zhang, *et al.*, Melatonin promotes the therapeutic effect of mesenchymal stem cells on type 2 diabetes mellitus by regulating TGF-β pathway, *Front. Cell Dev.*, 2021, **9**, 722365.

35 M. A. A. Ali, M. A. Nasser, A. N. Abdelhamid, I. A. A. Ali, H. S. Saudy and K. M. Hassan, Melatonin as a key factor for regulating and relieving abiotic stresses in harmony with phytohormones in horticultural plants — a review, *J. Soil Sci. Plant Nutr.*, 2023, **24**, 54–73.

36 M. Ding, N. Feng, D. Tang, J. Feng, Z. Li, M. Jia, *et al.*, Melatonin prevents Drp1-mediated mitochondrial fission in diabetic hearts through SIRT1-PGC1α pathway, *J. Pineal Res.*, 2018, **65**(2), e12491.

37 B. Li, Z. Zhang, H. Wang, D. Zhang, T. Han, H. Chen, *et al.*, Melatonin promotes peripheral nerve repair through Parkin-mediated mitophagy, *Free Radic. Biol. Med.*, 2022, **185**(20), 52–66.

38 Z. Qin, D.-D. Shi, W. Li, D. Cheng, Y.-D. Zhang, S. Zhang, *et al.*, Berberine ameliorates depression-like behaviors in mice *via* inhibiting NLRP3 inflammasome-mediated neuroinflammation and preventing neuroplasticity disruption, *J. Neuroinflamm.*, 2023, **20**(1), 54.

39 L. R. Wong, E. A. Tan, M. E. J. Lim, W. Shen, X. L. Lian, Y. Wang, *et al.*, Functional effects of berberine in modulating mitochondrial dysfunction and inflammatory response in the respective amyloidogenic cells and activated microglial cells – *in vitro* models simulating Alzheimer's disease pathology, *Life Sci.*, 2021, **282**(1), 119–824.

40 S. Sadraie, Z. Kiasalari, M. Razavian, S. Azimi, L. Sedighnejad, S. Afshin-Majd, *et al.*, Berberine ameliorates lipopolysaccharide-induced learning and memory deficit in the rat: insights into underlying molecular mechanisms, *Metab. Brain Dis.*, 2018, **34**(1), 245–255.

41 Z. An-Qi, L. Xiao-Yan, H. Ya-Ning, L. Bo-Hao, Z. Han-Lin, G. Jia-Hui, *et al.*, Improving interface properties of zein hydrolysis and its application in salad dressing through dispersion improvement assisted by potassium oleate aqueous solution, *Food Hydrocolloids*, 2022, **130**, 107–719.

42 L. Deng, X. Zhang, Y. Li, F. Que, X. Kang, Y. Liu, *et al.*, Characterization of gelatin/zein nanofibers by hybrid electrospinning, *Food Hydrocolloids*, 2018, **75**, 72–80.

43 F. Zheng, R. Li, Q. He, K. Koral, J. Tao, L. Fan, *et al.*, The electrostimulation and scar inhibition effect of chitosan/oxidized hydroxyethyl cellulose/reduced graphene oxide/asiaticoside liposome based hydrogel on peripheral nerve regeneration *in vitro*, *Biomater. Adv.*, 2019, **109**, 110–560.

44 L. Ling, W. Ning, J. Xun, D. Rui, N. Shihong, S. Lu, *et al.*, Biodegradable and injectable *in situ* cross-linking chitosan-hyaluronic acid based hydrogels for postoperative adhesion prevention, *Biomaterials*, 2014, **35**, 3903–3917.

45 J. Meng, G. Yang, L. Liu, Y. Song, L. Jiang and S. Wang, Cell adhesive spectra along surface wettability gradient from superhydrophilicity to superhydrophobicity, *Sci. China: Chem.*, 2017, **60**(5), 614–620.

46 B. Sun, W. Tong, J. Wang, D. Li, W. Jing, G. Qiang, *et al.*, Polypyrrole-coated poly(llactic acid-co-ε-caprolactone)/silk fibroin nanofibrous membranes promoting neural cells proliferation and differentiation with electrical stimulation, *J. Mater. Chem. B*, 2016, **4**, 6670–6679.

47 F. Safoora, M. Parinaz, S. Ali and B. Ali, Revitalizing the nervous system: exploring polypyrrole-based composites in nerve regeneration, *Mater. Today Commun.*, 2024, **41**, 110–685.

48 J. Liu, S. Lin, J. Dang, S. Wang, W. Cheng, Z. Ran, *et al.*, Anticancer and bone-enhanced nano-hydroxyapatite/gelatin/polylactic acid fibrous membrane with dual drug delivery and sequential release for osteosarcoma, *Int. J. Biol. Macromol.*, 2023, **240**, 124–406.

49 L. Jia, J. Liu, Z. Song, X. Pan, L. Chen, X. Cui, *et al.*, Berberine suppresses amyloid-beta-induced inflammatory response in microglia by inhibiting nuclear factor-kappaB and mitogen-activated protein kinase signalling pathways, *J. Pharm. Pharmacol.*, 2012, **64**(10), 1510–1521.